INTERNATIONAL JOURNAL FOR NUMERICAL METHODS IN FLUIDS
Int. J. Numer. Meth. Fluids 2002; **38**:963–984 (DOI: 10.1002/fld.250)

A stabilized finite element method for the Saint-Venant equations with application to irrigation

Guillermo Hauke*,†,‡

Departamento de Mecanica de Fluidos, Centro Politecnico Superior, C/Maria de Luna 3, 50015 Zaragoza, Spain

SUMMARY

When the two-dimensional shallow water equations are applied to solve practical irrigation problems, additional numerical difficulties arise. Large friction coefficients, dry bed conditions and singular infiltration terms engender new challenges which are addressed here to build a finite element method that is robust enough for this type of application. The proposed method is a stabilized formulation based on the symmetric quasi-linear form and the set of entropy variables. The robustness of the method is increased with a discontinuity capturing operator. A predictor multi-corrector algorithm is employed to solve the generalized trapezoidal rule. One of the novel features of the present technique is that an 'explicit' method has been developed with characteristics of implicit methods, so that the solution can be advanced at a convective CFL number of 1, regardless of the source terms. This leads to an economic procedure. Finally, an entropy production (in)equality is developed, which ensures the correct physical behaviour of the model and helps to determine the correct sign of the infiltration term. Copyright © 2002 John Wiley & Sons, Ltd.

KEY WORDS: finite elements; stabilized methods; shallow water; irrigation

1. INTRODUCTION

The Saint-Venant or shallow water equations are a simplified model of the Navier–Stokes equations for free surface flows. Although several assumptions apply, these equations find application in many practical flows such as dam-breaking waves, river floods, tidal waves and coastal currents. For these equations, a symmetric stabilized formulation based on the set of entropy variables has already been presented in References [1, 2] for both steady and

*Correspondence to: G. Hauke, Departamento de Mecanica de Fluidos, Centro Politecnico Superior, C/Maria de Luna 3, 50015 Zaragoza, Spain.
†E-mail: ghauke@posta.unizar.es
‡Professor Titular de Mecánica de Fluidos.

Contract/grant sponsor: Diputación General de Aragón (Spain); contract/grant number: PCA 1094
Contract/grant sponsor: Ministerio de Educación y Ciencia (Spain); contract/grant number: CICYT HID98-1099-C02-01

Received 3 April 2000
Revised 29 May 2001

unsteady computations. These methods incorporate all the experience acquired in stabilized finite element methods for the Navier–Stokes equations by discretely satisfying a generalized entropy production principle [3, 4]. In the above-mentioned references, the transient applications were dam-breaking/flood wave problems.

However, when these equations are applied to irrigation computation, additional numerical challenges are encountered which are not found in other situations. These challenges include (i) very small water levels h, (ii) advance and recession waves over a dry bed, where $h=0$, (iii) large friction coefficients and singular friction terms which become unbounded as $h\to 0$, (iv) very large, singular infiltration terms, and (v) a limitation on the CFL stability condition due to source terms.

All these factors make necessary the improvement of the method presented in Reference [2]. While increasing the robustness of the formulation, an 'explicit' method has been developed without restriction of the CFL number due to the source term, allowing for practical purposes a convective CFL $=1$, leading to an efficient and economic procedure.

An outline of the paper follows. In the first two sections, we review the shallow water equations for overland flow applications in their symmetric form and emphasize that their stability principle is the total energy equation for an isothermal flow. Some conclusions are drawn regarding the correct sign of the infiltration term. In the fourth section, we present the finite element formulation and the predictor multi-corrector algorithm employed to advance the equations in time. In the fifth section, practical computational details are outlined, and in the sixth several numerical examples are compared with other computations. Some conclusions end the paper.

2. THE SHALLOW WATER EQUATIONS FOR IRRIGATION APPLICATIONS

The shallow water equations can be expressed in conservative form as [5]

$$\mathbf{U}_{,t}+\mathbf{F}^{\mathrm{adv}}_{i,i}=\mathbf{S} \tag{1}$$

where $\mathbf{U}$ is the vector of conservation variables, $\mathbf{F}^{\mathrm{adv}}_i$ is the advective flux in the ith direction ($i=1,2$), and $\mathbf{S}$ is the source vector. An inferior comma represents partial differentiation and the summation convention on repeated indices is applied throughout.

Equation (1) has been written as a function of conservation variables,

$$\mathbf{U}=\begin{Bmatrix} U_1\\ U_2\\ U_3\end{Bmatrix}=h\begin{Bmatrix}1\\ u_1\\ u_2\end{Bmatrix} \tag{2}$$

where u_i are Cartesian velocity components and h is the water level with respect to the bed elevation z. The advective fluxes can be expressed as

$$\mathbf{F}^{\mathrm{adv}}_i=hu_i\begin{Bmatrix}1\\ u_1\\ u_2\end{Bmatrix}+\frac{1}{2}gh^2\begin{Bmatrix}0\\ \delta_{1i}\\ \delta_{2i}\end{Bmatrix} \tag{3}$$

which have been written as a function of g the gravity constant and δ_{ij} the Kronecker delta (the unit tensor, which takes on the value of 1 if $i=j$ and zero otherwise).

For overland flow applications, the source term includes three distinct contributions,

$$\mathbf{S} = \mathbf{S}_0 - \mathbf{S}_f + \mathbf{S}_{\text{inf}} \tag{4}$$

which represent, respectively, bottom slope, friction and infiltration.

Bottom slope, by means of bed elevation $z(x_1, x_2)$, can be expressed as

$$\mathbf{S}_0 = gh \begin{Bmatrix} 0 \\ \mathbf{S}_{o1} \\ \mathbf{S}_{o2} \end{Bmatrix} = -gh \begin{Bmatrix} 0 \\ z_{,1} \\ z_{,2} \end{Bmatrix} \tag{5}$$

Friction with the bed is modelled by the Manning friction law and, accordingly,

$$\mathbf{S}_f = gh \begin{Bmatrix} 0 \\ \mathbf{S}_{f1} \\ \mathbf{S}_{f2} \end{Bmatrix} = gh \frac{f^2 \sqrt{u_1^2 + u_2^2}}{h^{4/3}} \begin{Bmatrix} 0 \\ u_1 \\ u_2 \end{Bmatrix} \tag{6}$$

where f is the friction coefficient. Infiltration can be modelled by

$$\mathbf{S}_{\text{inf}} = \begin{Bmatrix} \mathbf{S}_{\text{inf}\,0} \\ \mathbf{S}_{\text{inf}\,1} \\ \mathbf{S}_{\text{inf}\,2} \end{Bmatrix} = \begin{Bmatrix} -i_{\text{inf}} \\ -\frac{1}{2} i_{\text{inf}} \;\; u_1 \\ -\frac{1}{2} i_{\text{inf}} \;\; u_2 \end{Bmatrix} \tag{7}$$

where i_{inf} is the infiltration rate, that is, the infiltrated volumetric flux per unit area, or $\mathrm{d}h_{\text{inf}}/\mathrm{d}t$, the infiltrated depth per unit time. In this work, this flux has been modelled by the Kostiakov–Lewis law [6]

$$\begin{aligned} i_{\text{inf}} &= \kappa a\, t_{\text{opp}}^{a-1} + i_0 \geqslant 0, \quad t_{\text{opp}} > 0 \\ i_{\text{inf}} &= 0, \qquad\qquad\qquad\quad t_{\text{opp}} \leqslant 0 \end{aligned} \tag{8}$$

where κ, a and i_0 are coefficients depending on soil properties. Here, t_{opp} is the 'opportunity time', the time during which the soil has been exposed to the liquid stream. There is some confusion in the literature about the sign of the infiltration term in the momentum equations. As will be proved later, in order to obey the principle of energy conservation, the correct signs are those displayed in Equation (7). This result is in accordance with Reference [6, Chapter 13].

Defining the generalized entropy function $\mathscr{H}(\mathbf{U})$ as the mechanical energy with respect to the bottom [7, 2],

$$\mathscr{H}(\mathbf{U}) = g \frac{h^2}{2} + h \frac{u_1^2 + u_2^2}{2} \tag{9}$$

the entropy variables are obtained by partial differentiation as

$$\mathbf{V} = \mathscr{H}_{,\mathbf{U}}^{\mathrm{T}} = \begin{Bmatrix} gh - \dfrac{u_1^2 + u_2^2}{2} \\ u_1 \\ u_2 \end{Bmatrix} \tag{10}$$

As a function of the entropy variables $\mathbf{V}$, the quasi-linear form of the system (1),

$$\tilde{\mathbf{A}}_0 \mathbf{V}_{,t} + \tilde{\mathbf{A}}_i \mathbf{V}_{,i} = \tilde{\mathbf{S}} \tag{11}$$

becomes a symmetric hyperbolic system [7, 2, 1]. That is, the coefficient matrices enjoy the special properties:

(i) $\tilde{\mathbf{A}}_0 = \mathbf{U}_{,\mathbf{V}}$ is symmetric, positive-definite.
(ii) $\tilde{\mathbf{A}}_i = \mathbf{F}^{\text{adv}}_{i,\mathbf{V}}$ is symmetric.

The explicit expression of these matrices can be found in Reference [2].

3. THE PRINCIPLE OF GENERALIZED ENTROPY PRODUCTION

As was pointed out in Reference [2], the principle of total energy conservation (which in this context of isothermal incompressible flow means the mechanical energy, i.e. kinetic plus potential energy with respect to z) is the *non-linear* stability principle of the Saint-Venant equations. It can be obtained from the system of equations by the dot product

$$\mathbf{V} \cdot (\mathbf{U}_{,t} + \mathbf{F}^{\text{adv}}_{i,i} - \mathbf{S}) = 0 \tag{12}$$

The analysis performed in Reference [2] is enlarged here to account for the infiltration term.

For any *smooth* solution, the different terms present in (12) can be expressed as follows:

$$\mathbf{V} \cdot \tilde{\mathbf{A}}_0 \mathbf{V}_{,t} = \mathscr{H}_{,\mathbf{U}} \cdot \mathbf{U}_{,t} = \mathscr{H}_{,t} \tag{13}$$

$$\mathbf{V} \cdot \mathbf{F}^{\text{adv}}_{i,i} = \left[u_i \left(gh^2 + \frac{1}{2} h|u|^2 \right) \right]_{,i} \tag{14}$$

$$\mathbf{V} \cdot \mathbf{S} = gh[(S_{oi} - S_{fi})u_i] + [S_{\text{inf}\,0} \;\; v_1 + S_{\text{inf}\,i} \;\; u_i] \tag{15}$$

The contribution due to infiltration can be rearranged to give

$$\begin{aligned} [S_{\text{inf}\,0} \;\; v_1 + S_{\text{inf}\,i} \;\; u_i] &= -\, i_{\text{inf}} \left[\left(gh - \frac{u_1^2 + u_2^2}{2} \right) + \frac{1}{2} (u_1^2 + u_2^2) \right] \\ &= -\, gh \;\; i_{\text{inf}} \\ &\leqslant 0 \end{aligned} \tag{16}$$

That is, the production of generalized entropy due to infiltration is *negative-semidefinite.* Gathering all the terms and simplifying yields

$$\begin{aligned} 0 = &[h(\tfrac{1}{2} gh + \tfrac{1}{2} |u|^2)]_{,t} \\ &+ [hu_i(gh + \tfrac{1}{2} |u|^2)]_{,i} \end{aligned}$$

$$+[gh\,z_{,i}\;\;u_i]$$
$$+[ghS_{fi}\;\;u_i]$$
$$+[ghi_{\inf}] \tag{17}$$

Integrating over the spatial domain Ω, and taking into account that the products $\mathbf{S}_{fi}u_i$ and $gh\,i_{\inf}$ are positive, one arrives at

$$\int_\Omega ([h(\tfrac{1}{2}\,gh+\tfrac{1}{2}\,|u|^2)]_{,t}+[hu_i(gh+\tfrac{1}{2}\,|u|^2)]_{,i}+[gh\,z_{,i}\;\;u_i])\,\mathrm{d}\Omega\leqslant 0 \tag{18}$$

That is, the mechanical energy, the sum of potential plus kinetic energy, must decrease, and it is a bounded function in the presence of appropriate boundary conditions.

If the sign of the infiltration term were

$$\mathbf{S}_{\inf}=\begin{Bmatrix} -i_{\inf} \\ +\tfrac{1}{2}\,i_{\inf}\;\;u_1 \\ +\tfrac{1}{2}\,i_{\inf}\;\;u_2 \end{Bmatrix} \tag{19}$$

which is frequently found in the literature, then

$$\begin{aligned}[S_{\inf 0}\;\;v_1+S_{\inf i}\;\;u_i] &= -i_{\inf}\left[\left(gh-\frac{u_1^2+u_2^2}{2}\right)-\frac{1}{2}\,(u_1^2+u_2^2)\right] \\ &= -i_{\inf}\left[gh-\frac{1}{2}\,(u_1^2+u_2^2)\right]\end{aligned} \tag{20}$$

which has an indefinite sign and does not guarantee energy boundness. In this case, the infiltration could *increase* the flow energy, which is not physically correct. In any case, for practical purposes, the sign of this term does not alter the solution significantly.

Introducing the definition of the entropy fluxes,

$$\sigma_i=hu_i(gh+\tfrac{1}{2}\,|\mathbf{u}|^2) \tag{21}$$

Equation (18) can also be written as

$$\int_\Omega (\mathscr{H}_{,t}+\sigma_{i,i}+[gh\;\;z_{,i}u_i])\,\mathrm{d}\Omega\leqslant 0 \tag{22}$$

Since the Hessian $\tilde{\mathbf{A}}_0^{-1}$ is positive-definite, $\mathscr{H}(\mathbf{U})$ is a convex function of the conserved properties and therefore, Equation (22) bounds the growth of the conservation variables themselves. Consequently, the principle of mechanical energy conservation is the stability statement of the shallow water equations and is also its *generalized entropy condition*.

This can be seen more clearly by making use of the continuity equation. Assuming that $z=z(x,y)$,

$$\begin{aligned}gh\;\;z_{,i}u_i &= (gh\;\;zu_i)_{,i}-z(gh\,u_i)_{,i} \\ &= (gh\;\;zu_i)_{,i}+(gh\,z)_{,t}\end{aligned} \tag{23}$$

which after substitution yields the principle of total energy conservation for an isothermal incompressible flow,

$$\begin{aligned}&\int_\Omega ([h(\tfrac{1}{2}gh+gz+\tfrac{1}{2}|\mathbf{u}|^2)]_{,t}+[hu_i(gh+gz+\tfrac{1}{2}|u|^2)]_{,i})\,\mathrm{d}\Omega\\&\quad=-\int_\Omega([ghS_{fi}\ \ u_i]+[gh_{\mathrm{inf}}])\,\mathrm{d}\Omega\\&\quad\leqslant 0\end{aligned}\tag{24}$$

4. FINITE ELEMENT FORMULATION

The system of equations based on the set of entropy variables is solved via the semi-discrete stabilized method introduced in Reference [2], which is improved and extended here to account for the infiltration term and large friction coefficients. Given an open spatial domain Ω with boundary Γ, subdivided into n_{el} elements with domain Ω^e, the weak form can be written as follows.

Given the solution at time t_n, find $\mathbf{V}\in\mathscr{S}$ such that $\forall\mathbf{W}\in\mathscr{V}$:

$$\begin{aligned}&\int_\Omega(\mathbf{W}\cdot\mathbf{U}_{,t}(\mathbf{V})-\mathbf{W}_{,i}\cdot\mathbf{F}_i^{\mathrm{adv}}(\mathbf{V})-\mathbf{W}\cdot\mathbf{S})\,\mathrm{d}\Omega\\&\quad+\sum_{e=1}^{n_{\mathrm{el}}}\int_{\Omega^e}\tilde{\mathscr{L}}\mathbf{W}\cdot\tilde{\boldsymbol{\tau}}(\tilde{\mathscr{L}}_t\mathbf{V}-\mathbf{S})\,\mathrm{d}\Omega\\&\quad+\sum_{e=1}^{n_{\mathrm{el}}}\int_{\Omega^e}\tilde{\nu}^h g^{ij}\mathbf{W}_{,i}\cdot\tilde{\mathbf{A}}_0\mathbf{V}_{,j}\,\mathrm{d}\Omega\\&\quad=-\int_\Gamma\mathbf{W}\cdot\mathbf{F}_i^{\mathrm{adv}}(\mathbf{V})n_i\,\mathrm{d}\Gamma\end{aligned}\tag{25}$$

The first and last integrals represent the Galerkin contributions, which have been integrated by parts for conservation. The second term is the Galerkin/least-squares integral, which adds stability to the method while retaining accuracy. Finally, the third integral is the discontinuity-capturing operator; a non-linear consistent operator that increases the control near discontinuities. Further details and notation of the method can be found in Reference [2] and references therein, which are completely necessary to fully understand this section.

The new procedure allows to take time steps at a CFL = 1 based on velocity, removing the stiff and complex source terms from stability considerations. It also allows a simpler computation of the friction terms as $h\to 0$. This technique departs from the previous version in the computation of the tangent matrix $\mathbf{M}^*$ employed in the predictor multi-corrector

algorithm [8, 9] (see Box 1 and Reference [2] for

Box 1. Predictor Multi-Corrector Algorithm.

(predictor phase)

$\mathbf{v}^{(0)} = \mathbf{v}^n$

(multi-corrector phase)

For $i = 0, 1, \ldots, i_{\max} - 1$

$\mathbf{M}^* \Delta \mathbf{v}^{(i)} = -\mathbf{R}^{(i)}$

$\mathbf{v}^{(i+1)} = \mathbf{v}^{(i)} + \Delta \mathbf{v}^{(i)}$

$\mathbf{v}^{n+1} = \mathbf{v}^{(i_{\max})}$

notation; in particular, $\mathbf{R}$ is the residual of the system of equations and $\mathbf{v}^{(i)}$ the nodal unknowns at iteration (i)).

The method is inspired on the following ideas. In 'explicit' finite element algorithms, the tangent matrix $\mathbf{M}^*$ is usually based only on the transient terms, typically the Galerkin mass matrix. However, this leads to an explicit treatment of the source terms which significantly reduces the time step allowed for stability. Source terms demand a selective treatment depending upon their sign. For unconditional stability, positive or production source terms should be treated explicitly, while negative or dissipative terms, implicitly. Therefore, the ideal algorithm should handle the source terms accordingly.

This concept is carried out in practice by a diagonally implicit treatment of the negative or dissipative source terms, whereas the positive source terms are left out from the tangent matrix, and thus are explicitly treated. To preserve the explicit structure of the algorithm, the dissipative contributions are lumped into the tangent matrix, $\mathbf{M}^*$. This diagonally lumped methodology has been observed to be sufficient for providing implicit character to the negative source terms. For a stability analysis of these methods, References [10, 11] can be consulted.

Depending on the choice of γ (the generalized trapezoidal rule parameter) and $i_{\max}$ (the number of corrector passes), different methods can be obtained. In particular, these are of special interest.

(i) A family of 'explicit' methods can be obtained by choosing the nodal blocks of $\mathbf{M}^* = [\mathbf{M}_{AB}]$ as

$$\mathbf{M}^*_{AB} = \left[\frac{1}{\Delta t} \int_\Omega N_A \tilde{\mathbf{A}}_0 N_B \, \mathrm{d}\Omega - \int_\Omega N_A \tilde{\mathbf{C}} N_B \, \mathrm{d}\Omega \right]^{\text{lumped}} \tag{26}$$

i.e. the lumped Galerkin mass–dissipation matrix. The tangent matrix for the dissipative source term $\tilde{\mathbf{C}}$ contains the friction and infiltration contributions and, in particular, is

written as

$$\tilde{\mathbf{C}} = \begin{bmatrix} -\dfrac{i_{\inf}}{gh} & 0 & 0 \\ 0 & -2\dfrac{f^2\sqrt{u_1^2+u_2^2}}{h^{1/3}} - \dfrac{1}{2}i_{\inf} & 0 \\ 0 & 0 & -2\dfrac{f^2\sqrt{u_1^2+u_2^2}}{h^{1/3}} - \dfrac{1}{2}i_{\inf} \end{bmatrix} \tag{27}$$

This tangent is almost the consistent tangent of the source term, but somewhat stiffer. With this choice, the resulting left-hand-side matrix is block-diagonal, and so the nodal diagonal blocks are inverted with a Cholesky decomposition which is guaranteed to exist because $\tilde{\mathbf{A}}_0 - \tilde{\mathbf{C}}$ is symmetric, positive-definite.

(ii) A family of implicit methods can be obtained by choosing

$$\begin{aligned} \mathbf{M}^*_{AB} = {} & \frac{1}{\Delta t}\int_\Omega N_A \tilde{\mathbf{A}}_0 N_B \,\mathrm{d}\Omega \\ & + \gamma \int_\Omega N_A \tilde{\mathbf{A}}_i N_{B,i} \,\mathrm{d}\Omega \\ & + \gamma \sum_{e=1}^{n_{\mathrm{el}}} \int_{\Omega^e} N_{A,i} \tilde{\mathbf{A}}_i \tilde{\boldsymbol{\tau}} \tilde{\mathbf{A}}_j N_{B,j} \,\mathrm{d}\Omega \\ & + \gamma \sum_{e=1}^{n_{\mathrm{el}}} \int_{\Omega^e} \tilde{v}^h g^{ij} N_{A,i} \tilde{\mathbf{A}}_0 N_{B,j} \,\mathrm{d}\Omega \\ & - \int_\Omega N_A \tilde{\mathbf{C}} N_B \,\mathrm{d}\Omega \end{aligned} \tag{28}$$

The same matrix $\tilde{\mathbf{C}}$ is chosen as before. Note the fully implicit treatment of the negative source terms. In this case, the linear system of equations is solved via the GMRES algorithm. (For more details, see Reference [9]).

Remarks

1. The 1-pass implicit method is equivalent to the 1-pass constant-in-time element of the space–time formulation, which is an excellent method for steady-state computations.
2. For transient calculations, the 'explicit' version is recommended with $\gamma = \frac{1}{2}$ and two corrector passes, i.e. $i_{\max} = 2$, which is second-order accurate in time.
3. For steady-state calculations, the implicit method is recommended with $\gamma = 1$ and one corrector pass, i.e. $i_{\max} = 1$, which is first-order accurate in time.

5. COMPUTATIONAL DETAILS

5.1. CFL number

Explicit algorithms are conditionally stable, and therefore there is a maximum allowable time step. The convective CFL number was evaluated based on velocity by means of the following expression

$$\mathrm{CFL} = \tfrac{1}{2}\Delta t \ \max(\sqrt{\alpha_s}(u+c), \sqrt{\alpha_n}c) \tag{29}$$

where

$$\begin{aligned} \alpha_s &= \xi_{i,s}\xi_{i,s} \\ \alpha_n &= \xi_{i,n}\xi_{i,n} \end{aligned} \tag{30}$$

are measures of the element size in the streamwise and orthogonal directions, respectively. Here ξ_k, $k = 1,2$, are the local element coordinates; s, the streamwise direction and n its normal.

5.2. Dry bed conditions

A very important practical situation is posed by what is called the *dry bed condition*, in which the initial water level h is zero. This causes computational

Box 2. Infiltration Rate Computation.

```
if t_opp ⩽ 0 or h ⩽ ε_inf then
    i_inf = 0
else
    i_inf = κ a t_opp^(a−1) + i_0
    i_inf = min(i_inf, ½ h/Δt)

endif
```

difficulties in many codes when h appears in the denominator. This problem has been solved by imposing a threshold value for the water level, the machine precision ε_{M},

$$h := \max(h, \varepsilon_{\mathrm{M}}) \tag{31}$$

Then, computations are carried out in all the elements without any exception.

Remark
With this new finite element method, the friction term does not need any specific treatment (compare with the method introduced in Reference [2], where the limit of h to zero in the friction term had to be carried out with care).

5.3. Computation of the infiltration term

Special care must be exercised with respect to the infiltration term if the Kostiakov–Lewis law is employed. When $t_{\mathrm{opp}} = 0$, the infiltration rate i_{inf} tends to infinity, which is not physically

correct since it does not account for the existing amount of water. Therefore, the following limit is imposed on $i_{\inf}$:

$$i_{\inf} := \min(i_{\inf}, \tfrac{1}{2}h/\Delta t)$$

The infiltration rate $i_{\inf}$ is assumed as time-dependent when applying the generalized trapezoidal rule.

The algorithm for the computation of the infiltration rate is displayed in Box 2.

5.4. Computation of the opportunity time

The opportunity time is interpolated with the same shape functions employed for the dependent variables and its computation is started when the front reaches a node (see Box 3). The front is detected by means of a threshold elevation $\varepsilon_{\inf}$, which is usually set to $\varepsilon_{\inf} = 0.001$ m (see for instance Reference [12]). There is some controversy regarding this approach but it is very simple and convenient.

Another choice found in the literature is to include a front detection algorithm.

Box 3. Opportunity Time Algorithm.

```
Initialize t_opp = 0 for each time step:
  if h > ε_inf then
    if t_opp = 0 then
        t_opp = ε_M
    else
        t_opp = t_opp + Δt
    endif
  endif
```

6. NUMERICAL EXAMPLES

First, two examples without infiltration are presented to show the good behaviour of the method after the modifications introduced in the present paper. Then three test cases including infiltration are presented, showing that in practical solutions, the new algorithm can in all cases advance the solution at a CFL = 1 based on velocity. This novel feature is lacked by standard numerical methods.

All the present simulations employed bilinear elements and were integrated with the standard 2×2 Gaussian quadrature rule.

6.1. Two-dimensional dam-break problem

This example consists of a dam-breaking test reported by the experimental data of Bellos *et al.* [13]. It consists of a gradually convergent–divergent channel of a total length of 21 m and a maximum width of 1.4 m, with a dam positioned at the narrowest section of the channel (width of 0.6 m and located at 8.5 m from the beginning). The channel is made of steel and consistently the friction of the bottom is modelled with a roughness coefficient of 0.012 [13].

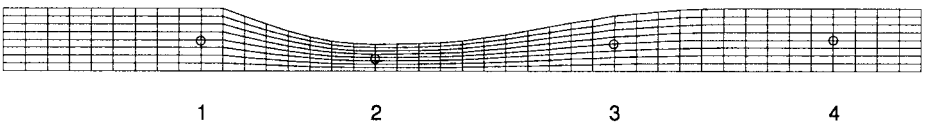

Figure 1. Two-dimensional dam-break problem. Mesh and probe positions.

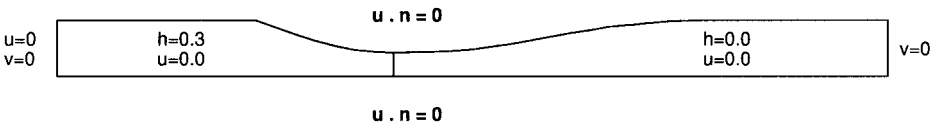

Figure 2. Two-dimensional dam-break problem. Problem set-up.

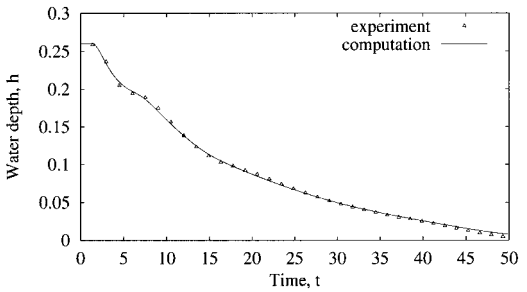

Figure 3. Two-dimensional dam-break problem. Water depth at station 1.

The mesh of 387 elements is shown in Figure 1. Circles show the position of stations where experimental data were gathered. Slip boundary conditions were set at the channel side walls, zero velocity at the beginning of the channel and zero vertical velocity component at the exit plane. See Figure 2. For the slip boundary conditions along the curved wall, in order to obtain a better representation of the normal vector to the boundary, the normal at each node was computed from the co-ordinates of the previous node and next node. This averaging process consistently improved the results. We consider here a dry bed test case with the initial conditions of $h = 0.3$ m at the left of the dam and $h = 0.0$ m at the right. The slope of the channel is 0.001 in this case.

The solution was advanced with a CFL number of 1. Results are plotted for the 'explicit' algorithm with $\gamma = \frac{1}{2}$ and $i_{\max} = 2$. Solutions were also computed with a halved mesh, of $16 \times 84 = 1344$ elements and 1445 nodes, which gave a similar solution, although slightly better resolved in zones of sharp changes.

Figures 3–6 show the water level as a function of time in four gauge positions. As can be seen, the water levels correlate very well with the experimental data during the entire time interval. Figure 7 shows three-dimensional pictures of the free surface at four consecutive times.

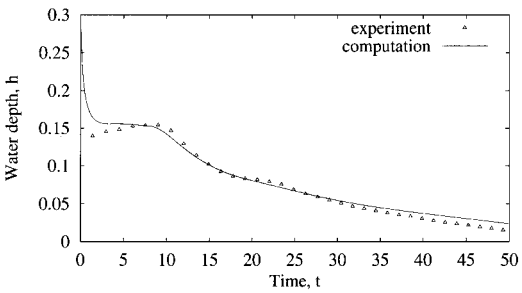

Figure 4. Two-dimensional dam-break problem. Water depth at station 2.

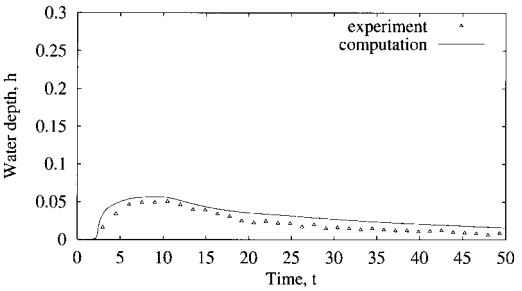

Figure 5. Two-dimensional dam-break problem. Water depth at station 3.

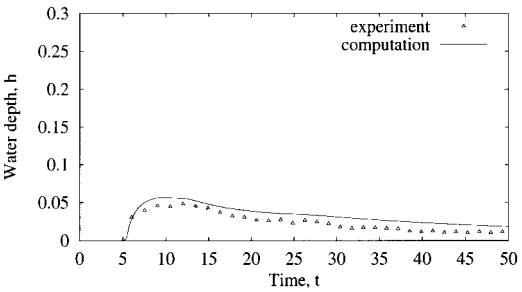

Figure 6. Two-dimensional dam-break problem. Water depth at station 4.

6.2. *Channel with sudden contraction*

This problem simulates the hydraulic jump caused by an instantaneous rupture of a dam in a symmetric channel with a sudden contraction. The channel has a total length of 18 m and a width of 0.5 m which becomes 0.2 m at the narrowest section. The dam is placed at $x = 0$. The experimental results were obtained by Bento [14]. The geometry, together with the position of the probes marked by circles, is depicted in Figure 8. The probes are located at the centre of the channel, at the co-ordinates $x = 6.1, 8.6, 10.5$ m.

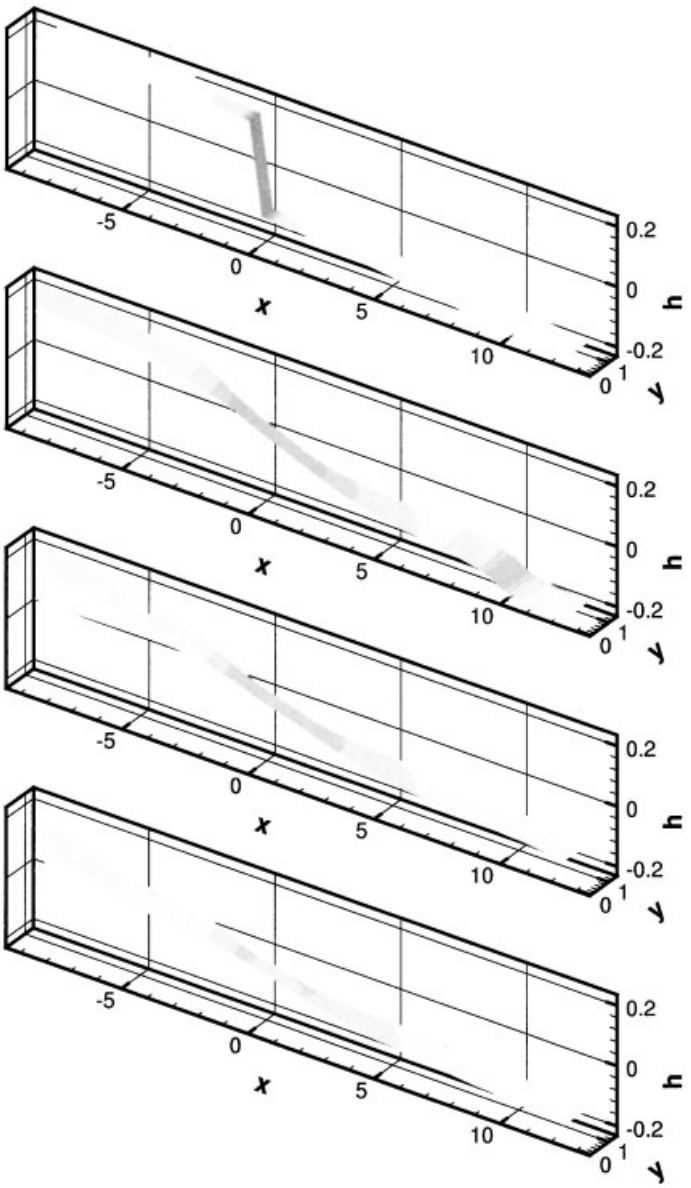

Figure 7. Two-dimensional dam-break problem. Free surface position at times $t = 0.0, 5.6, 11.8, 19.3$ s.

Because of the symmetry of the geometry, only half of the channel has been discretized. The elongated geometry and computational efficiency call for quadrilateral bilinear elements. Several meshes were considered: one of the 744 bilinear elements, formed by 8×93 quadrilaterals, and another of 1460 bilinear elements, formed by 10×146 quadrilaterals. In both

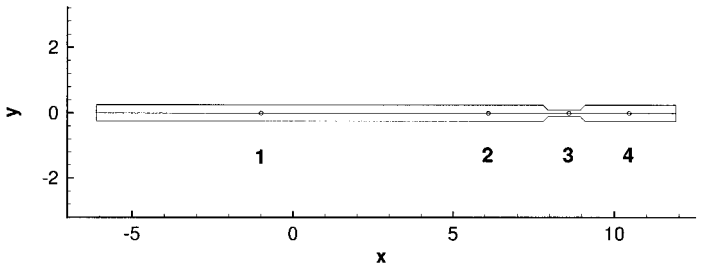

Figure 8. Channel with sudden contraction. Domain outline with probe positions.

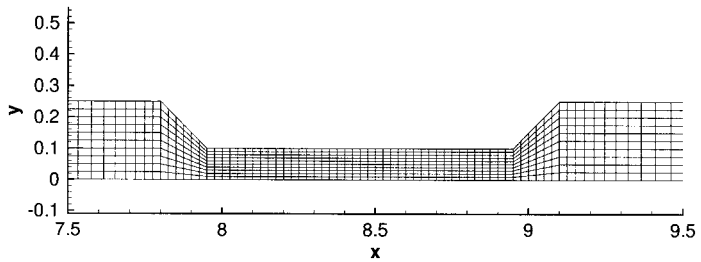

Figure 9. Channel with sudden contraction. Zoom of the mesh at contraction.

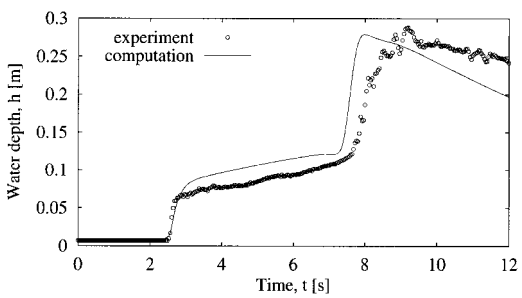

Figure 10. Channel with sudden contraction. Dry bed. Water depth at station 2.

cases, the elements were carefully stretched towards the converging section of the channel. In Figure 9, a zoom of the mesh near the contraction can be viewed.

The present case corresponds to the initial conditions of $h = 0.403$ m at the left of the dam and $h = 0.007$m at the right. The bottom of the channel has no slope. Slip boundary conditions were set at the channel side walls and at the symmetry line; zero velocity components at the beginning of the channel and zero vertical velocity component at the exit plane. The Manning friction coefficient employed was 0.011.

Results can be compared with the experimental data at the probes in Figures 10–12. The computed solution is within experimental scatter, and therefore behaves correctly, even though high vertical accelerations do occur near the entrance of the contraction. The elevation of the

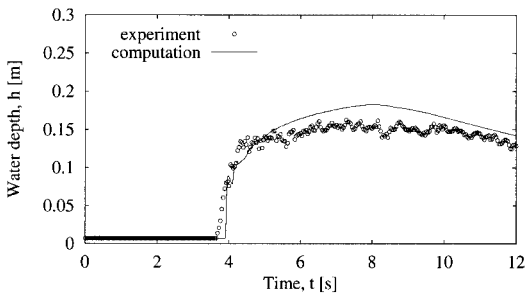

Figure 11. Channel with sudden contraction. Water depth at station 3.

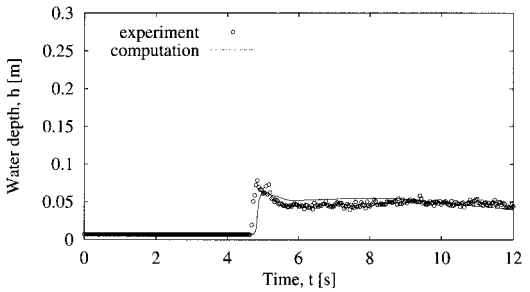

Figure 12. Channel with sudden contraction. Water depth at station 4.

water level can be observed in the 3D plots of Figures 13 and 14 for selected time steps. It can be observed how the wave front reaches the contraction, developing an upstream travelling hydraulic jump and stationary reflecting oblique jumps at the contraction exit.

6.3. *Parallel flow irrigation*

The next two examples consider the irrigation of a square field of side 100 m. In the first test case, the field is irrigated uniformly from the west side with a volumetric flow rate of $0.1\,\mathrm{m}^3/\mathrm{s}$. The orientation of the field with respect to the Cartesian co-ordinate system can be seen in Figure 15. The test case and the soil properties are taken from Reference [15], where soil friction and infiltration are given as $f = 0.14$, $a = 0.5$, $k = 0.006\,\mathrm{m\ min}^{-a}$, $i_0 = 0$.

Zero initial conditions are imposed in the whole domain. Boundary conditions are:

(i) Inlet (west side), $q = hu = 0.1/100\,\mathrm{m}^2/\mathrm{s}$.
(ii) Sides (north and south sides), $\mathbf{u} \cdot \mathbf{n} = 0$.
(iii) Exit (east side), none.

The solution was advanced in time with the explicit, second-order method, at a convective CFL of 1.

Results were obtained in several refined meshes of bilinear uniform elements. Here the results for the mesh with element sides of $\Delta x = 1.0\,\mathrm{m}$ are shown. In Figure 16, the present results

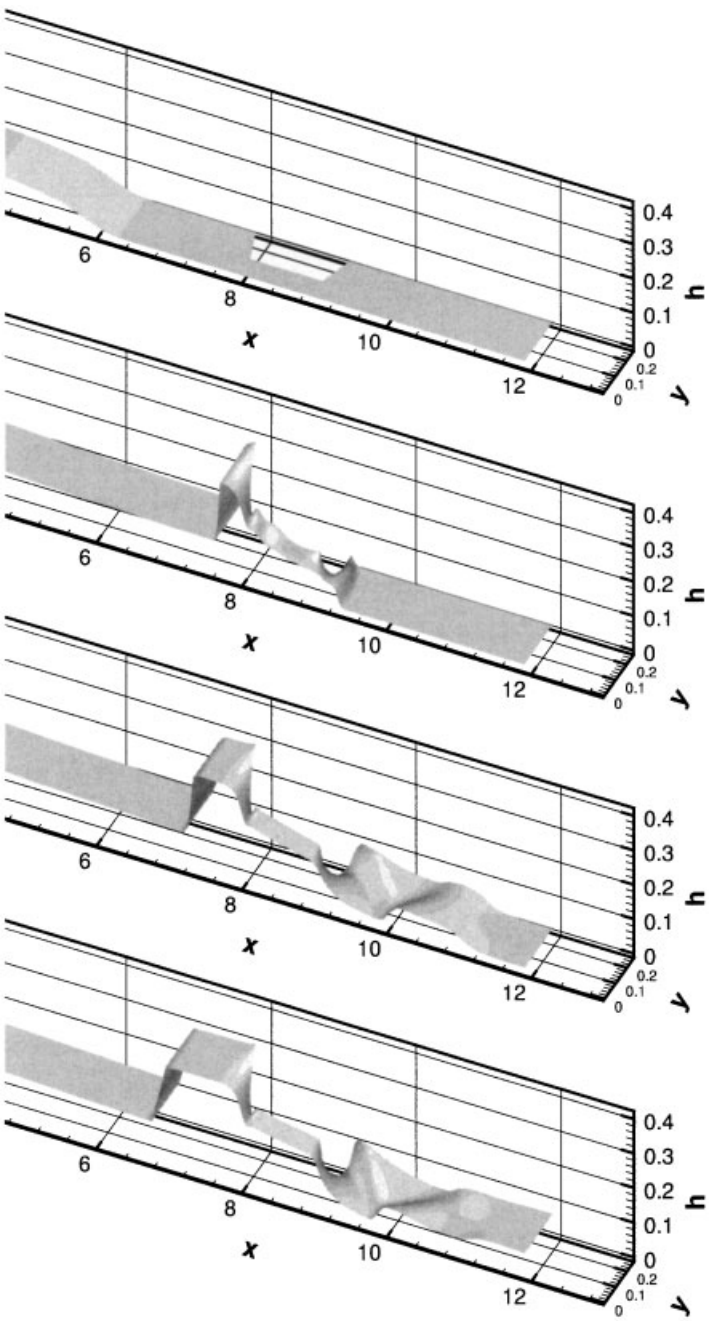

Figure 13. Free surface position at times $t = 2.51, 4.24, 5.12, 6.07$ s.

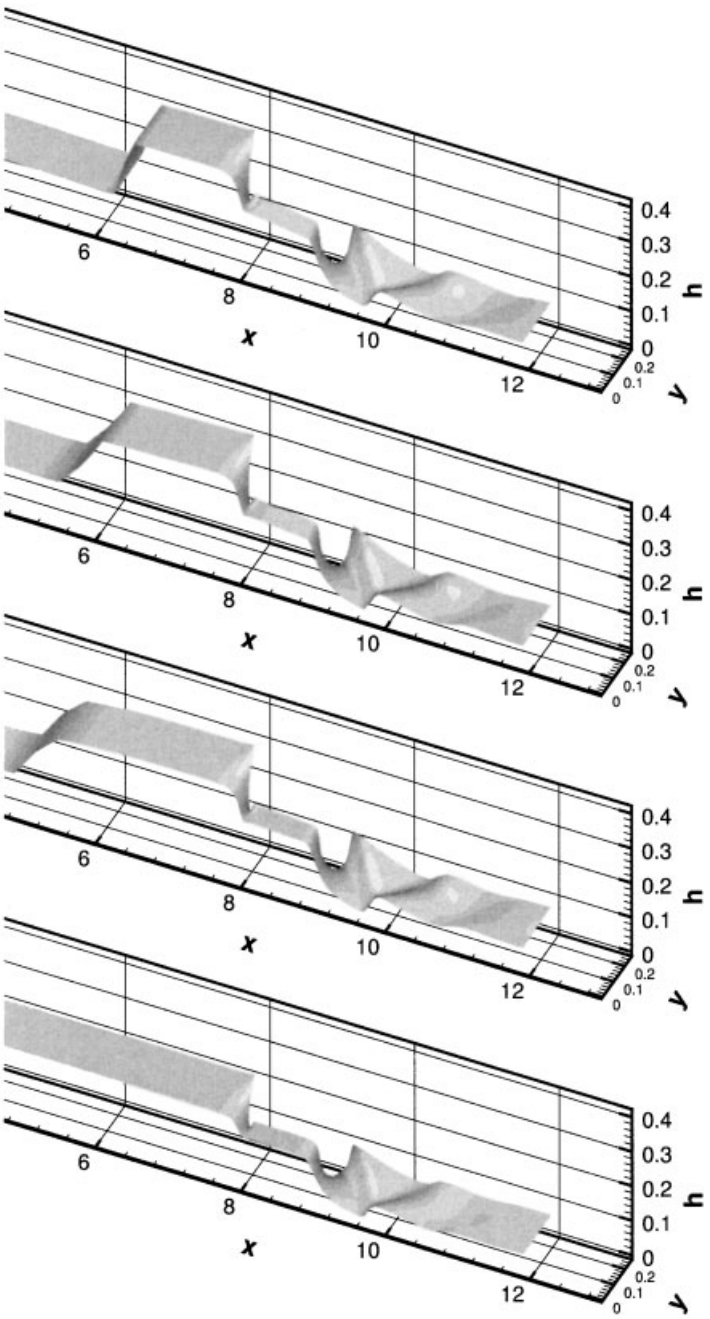

Figure 14. Free surface position at times $t = 7.03, 7.99, 8.97, 12.00$ s.

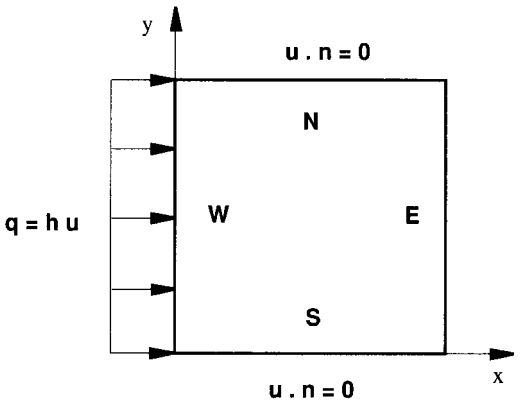

Figure 15. Parallel irrigation problem.

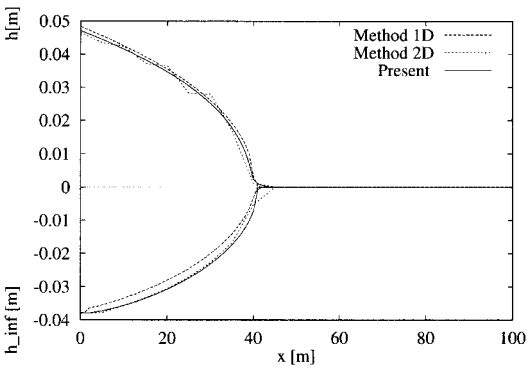

Figure 16. Water level and infiltrated depth at $t = 40$ min for parallel flow.

are compared with those of a one-dimensional finite volume method (referred as Method 1D) and of a bidimensional finite difference method (Method 2D), both reported in Reference [15]. The elevation of the water h is depicted in the positive portion of the vertical axis, whereas the infiltrated depth h_{inf} is shown in the negative portion of the plot. The results are displayed at the same time, $t = 40$ min. The present solution is stable, smooth and compares well with the solutions obtained by the other methods, with the advantage that the present method can be advanced at a CFL number of 1 based on velocity.

6.4. *Radial flow irrigation*

This example is similar to the previous one, but in this case the land is irrigated from the SW corner (see Figure 17). The boundary conditions are:

(i) Inlet, within the two elements at the SW corner, where the corresponding unitary flow $q = hu$ is imposed to give the total volumetric flux.

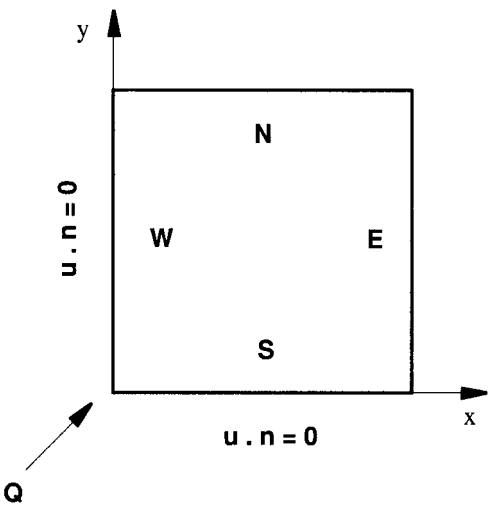

Figure 17. Radial irrigation problem.

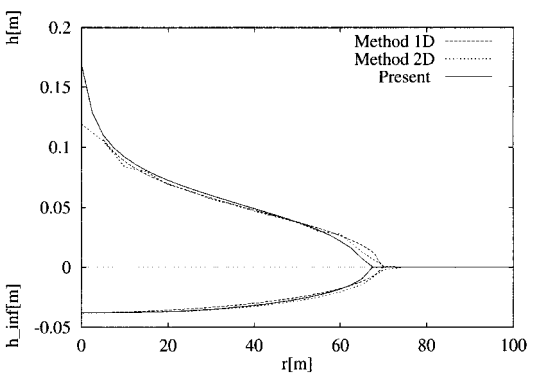

Figure 18. Water level and infiltrated depth at $t = 40$ min for radial flow.

(ii) West and south sides, slip boundary conditions.
(iii) Exit (north and east sides), none.

Solutions for a mesh of 40×40 bilinear elements are depicted in Figure 18 at time $t = 40$ min. Although in the present solution, the position of the front is lagged by one element, overall it compares very well with the one obtained by the other methods [15]. Again the method is able to advance the solution at a CFL $= 1$ based on velocity.

6.5. *Irrigation in microtopography*

This example simulates a real irrigation problem reported in Reference [16] as case Irrigation 2 by Zapata and Playan. The irrigated field is a square of side 27.0 m, whose microtopography

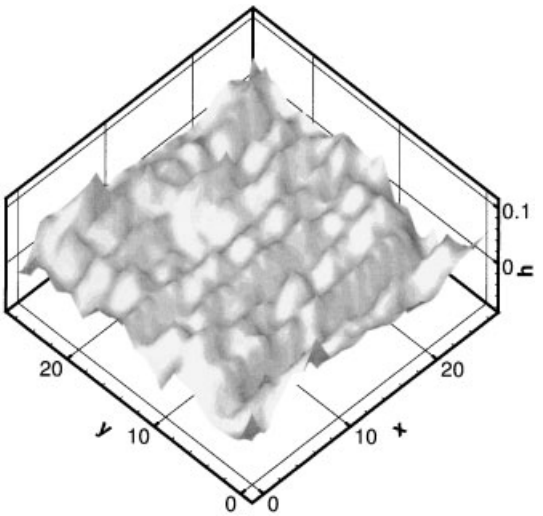

Figure 19. Ground topography for the case of microtopography.

is plotted in Figure 19. The field is irrigated with $0.0093\ \mathrm{m}^3/\mathrm{s}$ from the SW corner, i.e. the point with $(0,0)$ co-ordinates.

Two meshes have been employed. A mesh of 36×36 and another one of 54×54 bilinear elements, where the nodal co-ordinates coincide where the terrain elevation and infiltration depth were measured. The results shown are from the finer mesh. The boundary conditions are

(i) Inlet, within the two elements at the SW corner, where the corresponding unitary flow $q = hu$ is imposed to give the total volumetric flux of $0.0093\ \mathrm{m}^3/\mathrm{s}$.
(ii) Rest, slip boundary conditions.

Initial conditions were zero water elevation and zero velocity components everywhere. The friction and infiltration parameters, taken from Reference [16], are $f = 0.4$, $a = 0.2563$, $k = 0.01470\ \mathrm{m\ min}^{-a}$, and $i_0 = 0$.

The advancing front at the successive times $20, 40, 60, 80$ min can be seen in Figure 20 and a three-dimensional plot of the infiltrated depth at time 90 min in Figure 21. The solution compares very well with that reported in Reference [16]. Again, the robustness of the method allows to take time steps at a convective $\mathrm{CFL} = 1$.

7. CONCLUSIONS

A stabilized finite element method for the computation of irrigation applications has been presented. It is based on solving the shallow water equations by taking advantage of the symmetric hyperbolic form and the set of entropy variables. The solution in time is integrated via the generalized trapezoidal rule and a predictor multi-corrector method which takes special care of the source terms. An 'explicit' algorithm has been proposed which is capable of

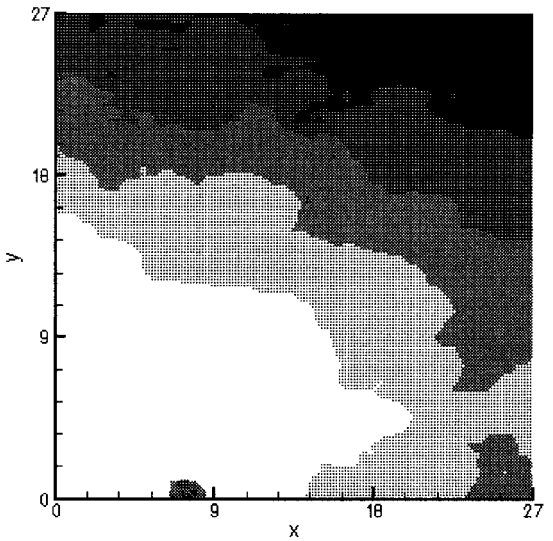

Figure 20. Advance curves for $t \approx 20, 40, 60, 80$ min.

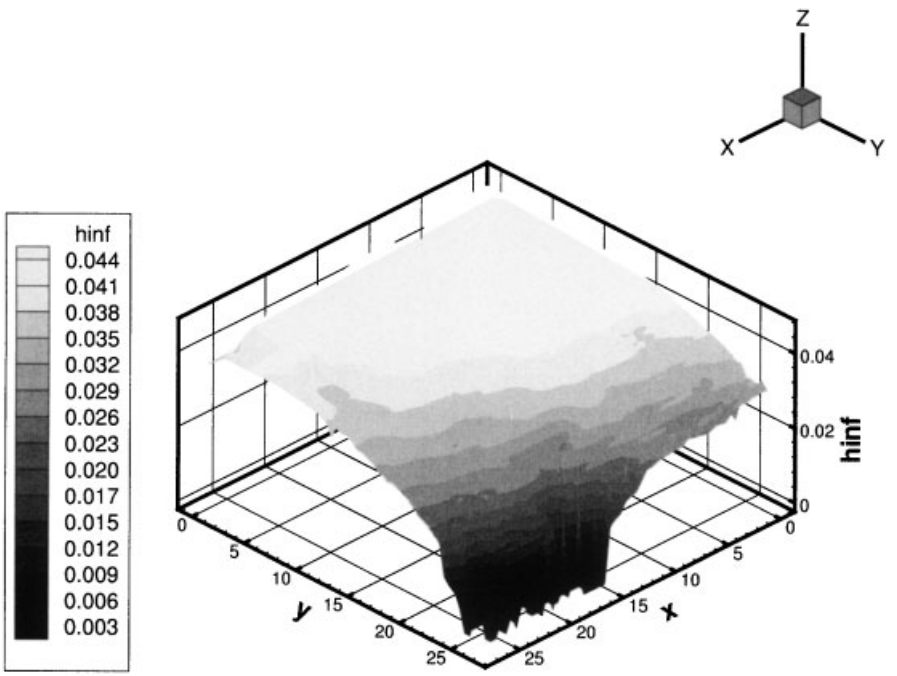

Figure 21. Infiltrated depth in metres at $t = 90$ min.

advancing the solution at a convective CFL number of 1, removing the source terms from stability considerations. This novel technique is based on a diagonal (lumped) implicit treatment of the negative source terms. The effectiveness of the procedure is shown on various problems, where the results are compared to experimental and other computational data.

ACKNOWLEDGEMENTS

This work has been partially funded by the Diputación General de Aragón (Spain) under the Contract PCA-1094 and the Ministerio de Educación y Ciencia under Contract CICYT HID98-1099-C02-01. The author acknowledges the helpful conversations with Enrique Playán, Neri Zapata and Pilar García-Navarro.

REFERENCES

1. Bova SW, Carey GF. An entropy variable formulation and applications for the two-dimensional shallow water equations. *International Journal for Numerical Methods in Fluids* 1996; **24**:29–46.
2. Hauke G. A symmetric formulation for computing transient shallow water flows. *Computer Methods in Applied Mechanics and Engineering* 1998; **163**:111–122.
3. Hauke G, Hughes TJR. A unified approach to compressible and incompressible flows. *Computer Methods in Applied Mechanics and Engineering* 1994; **113**:389–396.
4. Hauke G, Hughes TJR. A comparative study of different sets of variables for solving compressible and incompressible flows. *Computer Methods in Applied Mechanics and Engineering* 1998; **153**:1–44.
5. Vreugdenhil CB. *Numerical Methods for Shallow-Water Flow*. Kluwer Academic Publishers: Dordrecht, 1994.
6. Mahmood K, Yevjevich V. *Unsteady Flow in Open Channels*, vols. I and II. Water Resources Publications, Fort Collins, Colorado, 1975.
7. Tadmor E. Skew-selfadjoint form for systems of conservation laws. *Journal of Mathematical Analysis and Applications* 1984; **103**:428–442.
8. Brooks AN, Hughes TJR. Streamline upwind/Petrov–Galerkin formulations for convection dominated flows with particular emphasis on the incompressible Navier–Stokes equations. *Computer Methods in Applied Mechanics and Engineering* 1982; **32**:199–259.
9. Shakib F, Hughes TJR, Johan Z. A new finite element formulation for computational fluid dynamics: X. The compressible Euler and Navier–Stokes equations. *Computer Methods in Applied Mechanics and Engineering* 1991; **89**:141–219.
10. Hauke G. Fourier analysis of semi-discrete and space–time stabilized methods for the advective–diffusive–reactive equation. In preparation.
11. Hauke G, Lopez JL. Analysis of non-stationary finite element algorithms for overland flow computations. *ECCOMAS 2000*, Barcelona, 2000.
12. Playan E, Walker WR, Merkley GP. Two-dimensional simulation of basin irrigation. I: Theory. *Journal of Irrigation and Drainage Engineering* 1994; **120**:837–856.
13. Bellos CV, Soulis JV, Sakkas JG. Experimental investigation of two-dimensional dam-break induced flows. *Journal of Hydraulic Research* 1992; **30**:47–63.
14. Bento A. Modelação computacional e experimental de escoamentos provocados por roturas de barragens. *Ph.D. Thesis*, Universidad Técnica de Lisboa, 1996.
15. Playan E, Garcia-Navarro P. Radial flow modelling for estimating level-basin irrigation parameters. *Journal of Irrigation and Drainage Engineering* 1997; **123**:229–237.
16. Zapata N, Playan E. Simulating elevation and infiltration in level-basin irrigation. *Journal of Irrigation and Drainage Engineering* 2000; **126**:78–84.

